Dual Active Bridge Converter with AC Heating Capability for Lithium-ion Batteries in Electric Vehicles

Yuta Sasama
Department of Electrical and Electronic Engineering
Ibaraki University
Ibaraki, Japan
20nm624r@vc.ibaraki.ac.jp

Ryuichi Igarashi
Department of Electrical and Electronic Engineering
Ibaraki University
Ibaraki, Japan
18nm607n@vc.ibaraki.ac.jp

Masatoshi Uno
Department of Electrical and Electronic Engineering
Ibaraki University
Ibaraki, Japan
masatoshi.uno.ee@vc.ibaraki.ac.jp

***Abstract*—Lithium-ion batteries in electric vehicles need to be adequately heated at low temperatures to avoid the decrease in discharge capacity. AC heating techniques utilizing Joule heat generated by the internal resistance of batteries have been proposed. Although these techniques achieve higher heating efficiency and uniform heating, an ac heating inverter is separately necessary to produce the ac current, likely resulting in increased system complexity and cost. This paper proposes a dual active bridge (DAB) converter integrating an inverter for ac heating in electric vehicles. The proposed converter is derived by sharing two legs of both converters, achieving the simplified system and low-cost. Experimental results of a prototype with a charge-discharge power rating of 300 W demonstrated that in addition to the bidirectional power flow, the proposed converter heated up the twelve-cell battery from −11°C to 0°C within 10 min.**

Keywords— AC heating, dual active bridge (DAB) converter, internal resistance, lithium-ion battery, low temperature.

I. Introduction

In recent years, the electric vehicles (EVs) with zero carbon emission have drawn attention due to raising awareness of environmental issues. EVs are equipped with lithium-ion batteries (LIBs) with the advantages of high energy density and long life as their energy sources. However, the practical use at low temperatures faces a severe problem of increased internal resistance. Fig. 1 exemplifies the discharge characteristics of the LIB with the C/3 rate at four temperatures. The increased internal resistance under the subzero temperature condition significantly decreases the discharging voltage and time. The reduced discharging voltage and time result in a shortened driving distance, and therefore heating LIBs is necessary in cold areas.

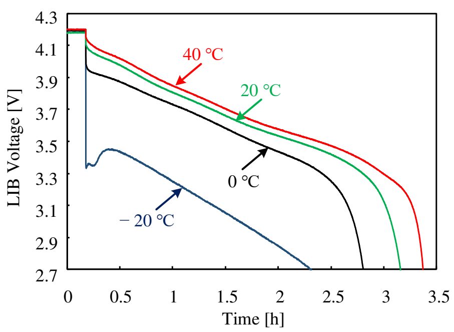

Fig. 1. Discharge characteristics of the LIB with C/3 rate at four temperatures.

A variety of heating methods have been proposed and are roughly divided into the external and internal heating techniques [1]–[3]. The LIB system using the external heating technique, such as electric heating wire with air or liquid as a heating medium, is illustrated in Fig. 2. This technique leads to the heat diffusion or nonuniform temperature distribution due to heat conduction and convection, resulting in the low heating efficiency or premature deterioration of LIBs.

To resolve these problems, internal heating techniques have been proposed [1]. Internal heating techniques utilize the Joule heat generated by current flowing through an internal resistance of LIBs. Compared with the external heating, the internal heating techniques achieve high heating efficiency thanks to the lack of heat conduction and convection process. Since the heat is generated from inside the LIB, the entire LIB can be heated uniformly.

Internal heating techniques can be classified into dc heating and ac heating. The difference between two methods in current

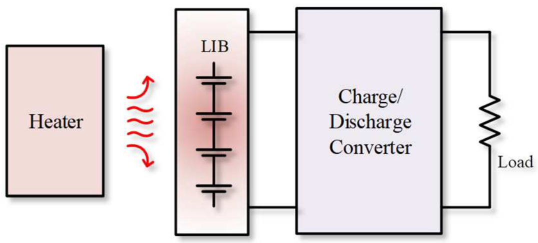

Fig. 2. LIB system using external heating techniques.

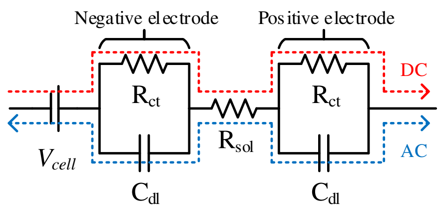

Fig. 3. Current flow directions at LIB using internal heating techniques.

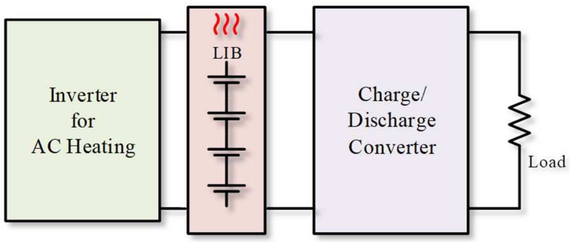

Fig. 4. LIB system using ac heating techniques.

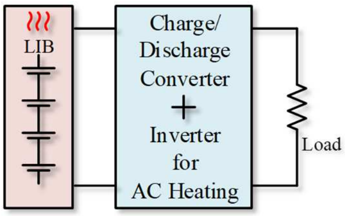

Fig. 5. Proposed LIB system.

flow directions in an equivalent circuit of a LIB is shown in Fig. 3. The equivalent circuit consists of the open-circuit voltage V_{cell}, the solvent resistance R_{sol}, the double-layer capacitance C_{dl}, and the charge-transfer resistance R_{ct}. A current flowing through R_{ct} contributes to the charge-discharge reactions of the LIB. The dc current flows through R_{ct}, and hence the dc heating techniques heat up LIBs with the charge-discharge reaction. However, the charge-discharge reaction at low temperatures brings about the premature deterioration or internal short circuit due to lithium deposition. On the other hand, the ac current with a frequency of a kHz or more flows through C_{dl} instead of R_{ct} due to almost zero reactance of C_{dl} [4]. Thus, ac heating techniques can heat up the LIB without charging or discharging [5], [6]. In conclusion, the ac current is more appropriate than the dc current to heat up the LIB in the internal heating technique.

The LIB system using the ac heating technique is illustrated in Fig. 4. This LIB system requires the inverter to generate the ac current in addition to the bidirectional converter that charge or discharge the LIB. The inverter includes multiple switching elements, and therefore the ac heating technique results in increased system complexity and cost [7].

In this paper, the bidirectional converter with ac heating capability is proposed. The proposed converter is derived from integration the dual active bridge (DAB) converter and ac heating inverter with sharing legs. Fig.5 shows the LIB system using the proposed converter. The integration of two converters reduces the total switch count, achieving the simplified system and low-cost.

This paper is organized as follows. Section II introduces the proposed converter and its major features. Section III presents the detailed operation analysis and mathematical modeling for the ac heating current. The experimental verification using the prototype with a charge-discharge power rating of 300 W will be presented in Section IV.

II. Proposed Converter

A. *Key Elements for Proposed Converter*

The topology using the series-resonant inverter, shown in Fig. 6(a), has been proposed as ac heating inverters for LIBs [6],

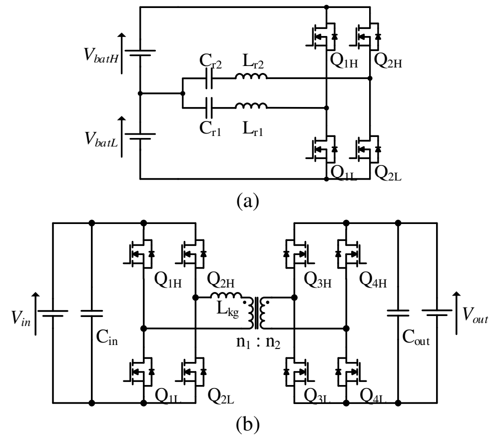

Fig. 6. Key elements. (a) Inverter for ac heating. (b) Dual active bridge (DAB) converter.

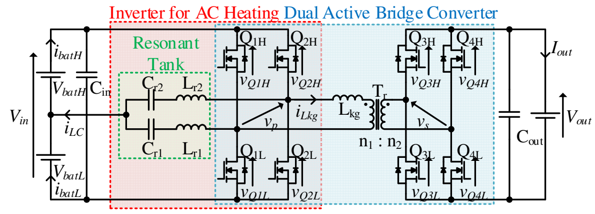

Fig. 7. Proposed converter.

[8]. This circuit consists of two legs of Q_{1H}-Q_{1L} and Q_{2H}-Q_{2L}, two resonant tanks C_{r1}-L_{r1} and C_{r2}-L_{r2}, and a battery divided into V_{batH} and V_{batL}. Resonant tanks are connected between the midpoint of V_{batH}-V_{batL}, Q_{1H}-Q_{1L} leg, and Q_{2H}-Q_{2L} leg.

This topology is equivalent to two single-phase series-resonant inverters connected in parallel, and therefore is suitable to enhance an ac heating current and to reduce the heating time. This inverter operates with a fixed 50% duty cycle d at a fixed switching frequency f_s without feedback control. Switching losses can be low due to zero current switching (ZCS).

The DAB converter, shown in Fig. 6(b), is identical to a traditional one. The DAB converter achieves bidirectional power flow by manipulating a phase shift (PS) angle between the primary and secondary winding voltages [9]. All switches can be driven in zero voltage switching (ZVS) manner in wide operating ranges.

B. *Configuration and Features*

Fig. 7 shows the proposed DAB converter. This converter is derived from integrating two converters shown in Fig. 6. In comparison with a conventional system using a bidirectional converter and ac heating inverter separately, not only can the system be simplified by the integration of two converters into a single unit, but also four switches are shared by both converters in the course of the integration, thus reducing the total switch count and cost.

The proposed converter operates either in the ac heating mode or power transfer mode. These two modes are with different principles at a different f_s and are independent of each other. The proposed converter operates with a ZCS and ZVS manner in the ac heating and power transfer mode, respectively, achieving soft-switching operations in both modes.

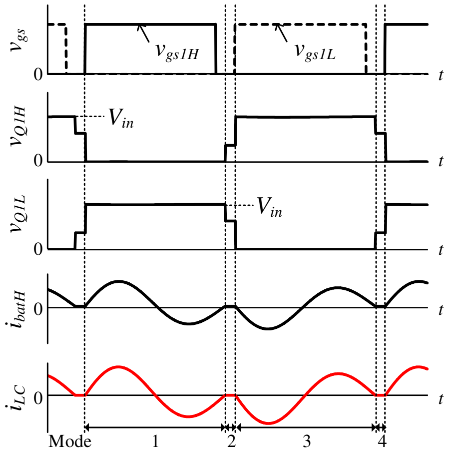

Fig. 8. Key operation waveforms in ac heating mode.

In the ac heating mode, f_s is a kHz-order. Only primary side switches are driven to generate the ac current i_{LC} by series-resonant tanks. The resonant frequency of the LC tanks f_r is set slightly higher than twice f_s to operate in discontinuous current mode (DCM). Resonant converters operating in the DCM are known to have constant current characteristics, realizing an over-current protection for batteries [10].

In the power transfer mode, on the other hand, f_s is several ten kHz-order. Similar to traditional DAB converters, all switches are driven. In this mode, f_s is set to be rather higher than f_r so that an impedance of LC tanks is high, and therefore, i_{LC} does not flow through LC tanks. The added LC tanks do not affect the power transfer operation, and the proposed converter operates similarly to the traditional one. Section III shows the details of two modes.

III. Operation Analysis

A. Operation Modes in AC Heating Mode

Theoretical operation waveforms and current flow directions in the ac heating mode are shown in Figs. 8 and 9, respectively. i_{batH} and i_{batL} are currents flowing through V_{batH} and V_{batL}. It should be noted that high-side switches Q_{1H} and Q_{2H} synchronize, and so do low-side switches Q_{1L} and Q_{2L}.

Mode 1 [Fig. 9(a)]: The gating signals for the high-side switches, v_{gs1H} and v_{gs2H}, are applied at i_{LC} = 0, achieving ZCS turn-on. Voltages of the resonant tanks, v_{LC1} and v_{LC2}, equal to V_{batH}, and i_{LC} flows. i_{LC} splits into i_{batH} and i_{batL} that translate into Joule heat to heat up V_{batH} and V_{batL}, respectively. The primary winding is short-circuited through Q_{1H} and Q_{2H}, and its voltage v_p is zero. Gating signals of v_{gs1H} and v_{gs2H} are removed before i_{LC} becomes zero again. Body diodes conduct after Q_{1H} and Q_{2H} turn off, achieving ZVS turn-off.

Mode 2 [Fig. 9(b)]: This mode begins as i_{LC} reaches zero. The current flows through only the capacitor C_{in}.

Mode 3 [Fig. 9(c)]: The gating signals for the low-side switches, v_{gs1L} and v_{gs2L}, are applied at i_{LC} = 0, achieving ZCS turn-on. v_{LC1} and v_{LC2} equal to V_{batH}, and i_{LC} flows. The primary winding is short-circuited through Q_{1L} and Q_{2L}, and v_p is zero. Gating signals of v_{gs1L} and v_{gs2L} are removed before i_{LC} becomes zero similarly to Mode 1. Body diodes conduct after Q_{1L} and Q_{2L} turn off, achieving ZVS turn-off.

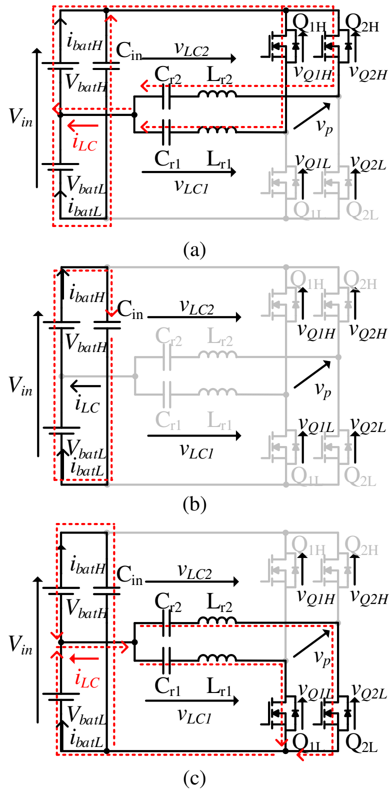

Fig. 9. Current flow directions in ac heating mode. (a) Mode 1, (b) Mode 2 and 4, and (c) Mode 3.

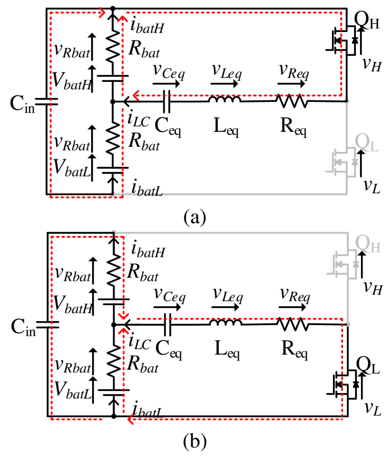

Fig. 10. Equivalent circuits in ac heating mode. (a) Mode 1 and (b) Mode 3.

Mode 4 [Fig. 9(b)]: This mode is identical to Mode 2, and hence i_{LC} is zero.

In summary, v_p is zero at all times throughout the switching cycle. Thus, this converter can heat up the LIB without transferring power to the secondary side. Besides, all switches achieve ZCS turn-on and ZVS turn-off.

B. Resonant Current

This section analyzes i_{LC}. Modes 2 and 4 can be neglected because i_{LC} is always zero. For the analysis, equivalent circuits in the ac heating mode are shown in Fig. 10. To simplify the analysis, two resonant tanks are combined into one in this equivalent circuit. R_{eq}, L_{eq}, and C_{eq} (as designated in Fig. 10) are given by

$$R_{eq} = R_L + R_C + R_{on} \tag{1}$$

$$L_{eq} = \frac{L_{r1}L_{r2}}{L_{r1} + L_{r2}} \tag{2}$$

$$C_{eq} = C_{r1} + C_{r2} \tag{3}$$

where R_{on} is on resistances of switches, and R_L and R_C are equivalent series resistances of the inductor and capacitor, respectively. The resonant frequency of the RLC series circuit, which consists of R_{eq}, L_{eq}, and C_{eq}, is expressed as

$$f_r = \frac{1}{2\pi\sqrt{L_{eq}C_{eq}}} \tag{4}$$

When V_{batH} and V_{batL} have the same characteristics and $i_{LC}(t)$ evenly splits, $i_{batH}(t)$ and $i_{batL}(t)$ are given by

$$i_{batH}(t) = -i_{batL}(t) = \frac{1}{2}i_{LC}(t) \tag{5}$$

From Fig. 10(a),

$$\begin{aligned} V_{batH} &= -v_{Rbat} + v_{Req} + v_{Leq} + v_{Ceq} \\ &= \left(R_{eq} - \frac{1}{2}R_{bat}\right)i_{LC} + L_{eq}\frac{di_{LC}}{dt} \\ &\quad + \frac{1}{C_{eq}}\int i_{LC}dt \end{aligned} \tag{6}$$

where R_{bat} is the internal resistance of the battery, and v_{Rbat}, v_{Req}, v_{Ceq}, and v_{Leq} are voltages of R_{bat}, R_{eq}, C_{eq}, and L_{eq}, respectively. To simplify the analysis, γ and ω are defined as

$$\gamma = \frac{2R_{eq} - R_{bat}}{4L_{eq}} \tag{7}$$

$$\omega = \sqrt{\frac{1}{L_{eq}C_{eq}} - \gamma^2} \tag{8}$$

According to (6), $i_{LC}(t)$ in Mode 1 is deduced as

$$i_{LC}(t) = \frac{V_{batH} + v_{Ceq}(0)}{\omega L_{eq}} \cdot e^{-\gamma t} \cdot sin\omega t \tag{9}$$

where $v_{Ceq}(0)$ is the initial value of v_{Ceq}. ω should be positive for an underdamped oscillation in the current wave, and therefore C_{eq} and L_{eq} have to meet the following requirement.

$$\frac{1}{L_{eq}C_{eq}} - \gamma^2 > 0 \tag{10}$$

Similar to (9), $i_{LC}(t)$ in Mode 3 is given by

$$i_{LC}(t) = \frac{-V_{batL} + v_{Ceq}(0)}{\omega L_{eq}} \cdot e^{-\gamma t} \cdot sin\omega t \tag{11}$$

According to (9) and (11), the coefficient and γ determine the peak value and attenuation, respectively. I_{batH} and I_{batL}, the RMS values of $i_{batH}(t)$ and $i_{batL}(t)$, are expressed as

$$I_{batH} = I_{batL} = \sqrt{\frac{1}{T_s} \cdot \int_0^{T_s} i_{batH}{}^2(t)} \tag{12}$$

where T_s is the switching period. The Joule heat, Q_{batH} and Q_{batL}, which heat up V_{batH} and V_{batL}, can be yield by (12) as

$$Q_{batH} = Q_{batL} = R_{bat} \cdot I_{batH}{}^2 \cdot t \tag{13}$$

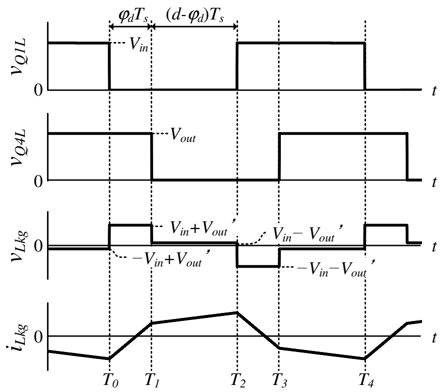

Fig. 11. Key operation waveforms in power transfer mode.

According to (13), the larger the values of I_{batH} and I_{batL}, the shorter will be the heating time.

C. Operation Modes in Power Transfer Mode

The power transfer direction from the primary to secondary side is defined as discharging operation, and vice versa. Theoretical operation waveforms in the discharging operation are shown in Fig. 11. φ is the PS angle between Q_{1H}-Q_{1L} and Q_{4H}-Q_{4L}, and φ_d is the PS duty cycle (= φ/360°). d is fixed to be 50% to maximize the amount of power transfer, and T_d is assumed short enough to be neglected. V_{in} and V_{out}' are defined as

$$V_{in} = V_{batH} + V_{batL} \tag{14}$$

$$V_{out}' = \frac{n_1}{n_2}V_{out} \tag{15}$$

As mentioned in the previous section, the proposed converter operates identically to the traditional ones [11]–[13] when f_s is rather higher than f_r. The output current of the DAB converter I_{out} can be expressed in the identical form,

$$\begin{aligned} I_{out} &= \frac{2}{T_s}\frac{V_{in}}{V_{out}}\int_{T_0}^{T_2} i_{Lkg}dt \\ &= \frac{V_{in}}{L_{kg}f_s}\frac{n_1}{n_2}\varphi_d(1 - |2\varphi_d|) \end{aligned} \tag{16}$$

where L_{kg} is the transformer leakage inductance, and i_{Lkg} is the current of L_{kg}.

The output power P_{out} is given by

$$\begin{aligned} P_{out} &= I_{out} \cdot V_{out} \\ &= \frac{V_{in}V_{out}}{L_{kg}f_s}\frac{n_1}{n_2}\varphi_d(1 - |2\varphi_d|) \end{aligned} \tag{17}$$

Therefore, I_{out} and P_{out} can be controlled by manipulating φ_d.

IV. Experimental results

A. Prototype

A prototype with a charge-discharge power rating of 300 W was designed for a LIB consisting of twelve cells connected in series, as shown in Fig. 12, and its component values are listed in Table I. V_{in} and V_{out} were 48 V and 200 V. f_s was set to be 2.5kHz and 50 kHz in the ac heating mode and power transfer mode, respectively. f_r was 5.4kHz to achieve the DCM operation in the ac heating mode, as mentioned in section II-B.

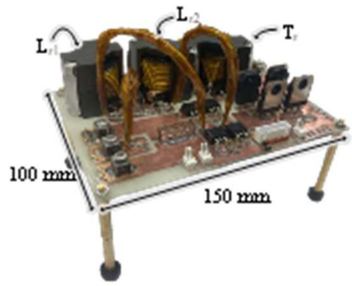

Fig. 12. Photographs of prototype with a charge-discharge power rating of 300 W.

TABLE I. COMPONENT VALUES

Component	Symbol	Value
Switch	Q_{1H}, Q_{2H}, Q_{1L}, Q_{2L}	FDB110N15A, R_{on} = 11 mΩ
	Q_{3H}, Q_{4H}, Q_{3L}, Q_{4L}	IXFX98N50P3, R_{on} = 50 mΩ
Capacitor	C_{r1}, C_{r2}	Ceramic capacitor, 15 µF
	C_{in}	Ceramic capacitor, 15 µF×12
	C_{out}	Aluminum electrolytic capacitor, 220 µF
Inductor	L_{r1}, L_{r2}	57 µH
	L_{kg} (transformer)	1 µH
	L_{kg} (auxiliary)	13 µH
Transformer	T_r	$n_1 : n_2$ = 3 : 13

B. LIB Heating

Fig. 13 shows the experimental platform using the thermostatic chamber for LIB heating. The initial LIB temperature was set to be −11°C. Fig. 14 shows measured key operation waveforms in the ac heating mode. These waveforms agreed well with the theoretical ones shown in Fig. 8, verifying the DCM operation of the prototype.

Fig. 15 shows the temperature evolution of the LIB. The LIB temperature rose to 0°C within 10 min. Fig. 16 shows the temperature distributions of the LIB before and after heating. Fig. 16(b) shows that the LIB temperature was uneven. The result implies that the heat radiation was not even by convection in the thermostatic chamber, and the unevenness was not caused by the ac heating operation.

C. Power Transfer

The power transfer test was conducted using a dc power supply and an electric load instead of the LIB. Large-capacity electrolytic capacitors were connected to the midpoint between resonant tanks and batteries. To investigate the impact of resonant tanks, power conversion efficiencies of the DAB converter alone were also measured by removing resonant tanks.

Fig. 17 shows the measured key operation waveforms at 300 W in the power transfer mode. These waveforms agreed well with the theoretical ones shown in Fig. 11, verifying the operation of the prototype. i_{LC} was considerably smaller than i_{Lkg}, demonstrating the power transfer without the current flowing through resonant tanks.

Fig. 18 shows drain-source and gate-source voltages of Q_{1H}-Q_{1L} and Q_{4H}-Q_{4L}, v_{ds} and v_{gs}, at 300 W in the discharge operation. v_{gs} was applied after v_{ds} declined to zero, verifying ZVS turn-on. Although only some waveforms are shown due to space

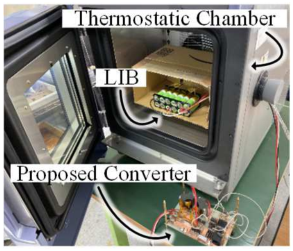

Fig. 13. Experimental platform using thermostatic chamber for LIB heating.

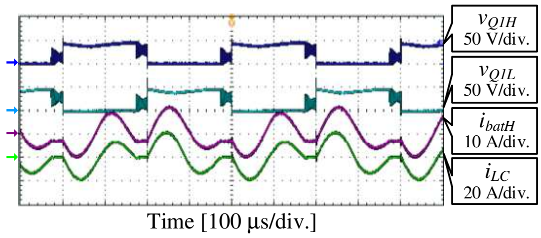

Fig. 14. Measured key waveforms in ac heating mode.

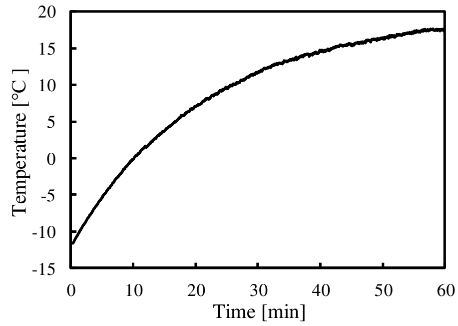

Fig. 15. Temperature evolution of the LIB surface.

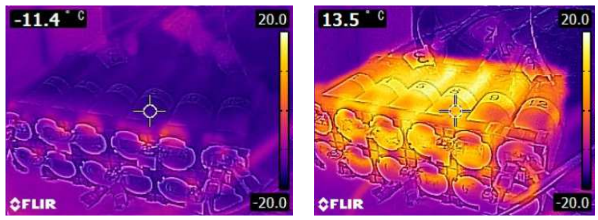

(a) (b)

Fig. 16. Temperature distributions (a) before heating and (b) after heating for 60 minutes.

limitations, ZVS turn-on for all switches were achieved in both discharging and charging operation.

Fig. 19 shows measured characteristics of P_{out} as a function of φ_d. P_{out} reached a rated power of 300 W at φ_d = 0.167, and the measured characteristics agreed well with the theoretical ones. These results demonstrated the direction of power transfer and the amount of output power could be controlled by manipulating φ_d.

Fig. 20 shows the measured power conversion efficiencies in the discharging operation. The efficiency of the traditional DAB converter was 90.7% at 300 W, while that of the proposed one was 90.4%. This result verifies the impact of the added resonant tank on the power conversion efficiency of the proposed DAB converter was very minor.

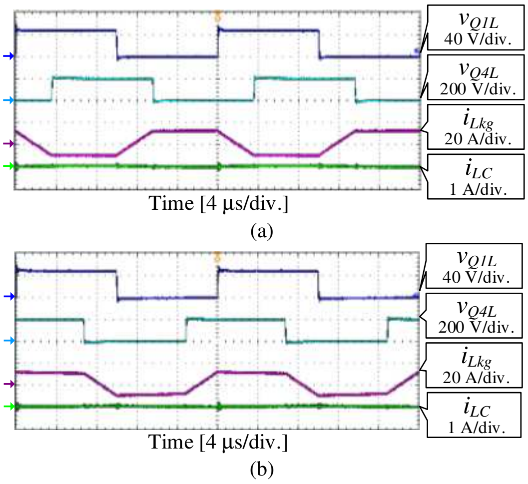

Fig. 17. Measured key waveforms at 300 W in power transfer mode. (a) The discharge operation. (b) The charge operation.

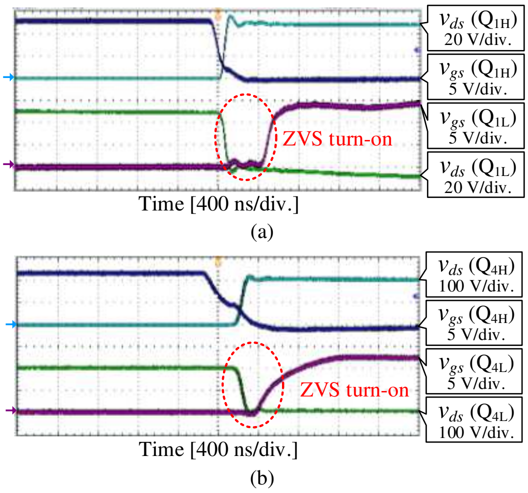

Fig. 18. ZVS waveforms at 300 W in power transfer mode. (a) Q_{1L} turn-on. (b) Q_{4L} turn-on.

V. Conclusions

This paper has proposed the DAB converter with ac heating capability for LIBs in EVs. The proposed converter is derived from the integration of two converters with sharing switches, achieving the simplified system and low-cost. The proposed converter operates either in the ac heating mode or the power transfer mode.

The detailed operation analysis and mathematical modeling for the ac current were conducted. The experimental verification demonstrated that the prototype could heat the twelve-cell LIB from −11°C to 0°C within 10 min by ac heating, in addition to the bidirectional power flow by the DAB converters.

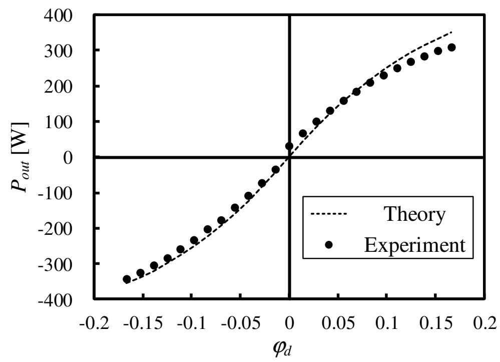

Fig. 19. Measured characteristics of P_{out} as a function of φ_d.

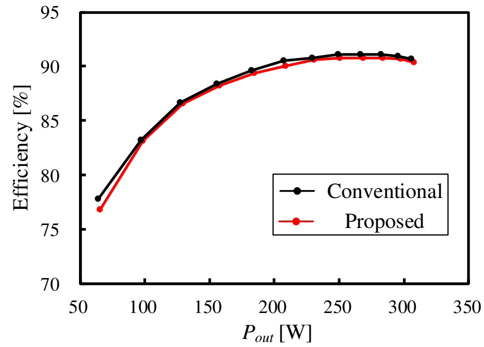

Fig. 20. Measured power conversion efficiencies.

References

[1] Y. Ji and C. Y. Wang, "Heating strategies for Li-ion batteries operated from subzero temperatures," *Electrochimica Acta*, vol. 107, pp. 664–674, Sep. 2013.

[2] T. A. Stuart and A. Hande, "HEV battery heating using AC currents," *Journal of Power Sources*, vol. 129, pp. 368–378, Apr. 2004.

[3] Z. G. Qu, Z. Y. Jiang, and Q.Wang, "Experimental study on pulse self-heating of lithium-ion battery at low temperature," *Int. J. Heat and Mass Transfer*, vol. 135, pp. 696–705, Jun. 2019.

[4] A. Jossen, "Fundamental of battery dynamics," *Journal of Power Sources*, vol. 154, pp. 530–538, Mar. 2006.

[5] J. Zhang, H. Ge, Z. Li, and Z. Ding, "Internal heating of lithium-ion batteries using alternating current based on the heat generation model on frequency domain," *Journal of Power Sources*, vol. 273, pp. 1030–1037, Jan. 2015.

[6] J. Jiang, H. Ruan, B. Sun, L. Wang, W. Gao, and W. Zhang, "A low-temperature heating strategy without lifetime reduction for large-size automotive lithium-ion battery pack," *Applied Energy*, vol. 230, pp. 257–266, Nov. 2018.

[7] Y. Shang, B. Xia, N. Cui, C. Zhang, and C. C. Mi, "An automotive onboard ac heater without external power supplies for lithium-ion batteries at low temperatures," *IEEE Trans. Power Electron.*, vol. 33, pp. 7759–7769, Sep. 2018.

[8] Y. Shang, K. Liu, N. Cui, Q. Zhang, and C. Zhang, "A sine-wave heating circuit for automotive battery self-heating at subzero temperatures," *IEEE Trans. Ind. Informatics*, vol. 16, pp. 3355–3365, May 2020.

[9] R. W. De Doncker, D. M. Divan, and M.H. Kheraluwala, "A three-phase soft-switched high power density dc/dc converter for high power applications," *IEEE, Trans. Ind. Appl.*, vol. 27, pp. 63–73, Jan./Feb. 1991.

[10] M. Uno and A. Kukita, "Bidirectional PWM converter integrating cell voltage equalizer using series-resonant voltage multiplier for series-connected energy storage cells," *IEEE Trans. Power Electron.*, vol. 32, pp. 8500–8513, Nov. 2017.

[11] X. Liu, Z. Q. Zhu, David A. Stone, Martin P. Foster, W. Q.Chu, Iain Urquhart, and James Greenough, "Novel dual-phase-shift control with bidirectional inner phase shifts for a dual-active bridge converter having low surge current and stable power control," *IEEE Trans. Power Electron.*, vol. 32, pp.4095–4106, May 2017.

[12] W. Song, N. Hou, and M. Wu, "Virtual direct power control scheme of dual active bridge DC–DC converters for fast dynamic response," *IEEE Trans. Power Electron.*, vol. 33, pp.1750–1759, Feb. 2018.

[13] Z. Qin, Y. Shen, P. C. Loh, H. Wang, and F. Blaabjerg, "A dual active bridge converter with an extended high-efficiency range by DC blocking capacitor voltage control," *IEEE Trans. Power Electron.*, vol. 33, pp.5949–5966, Jul. 2018